Desalination and Water Treatment
www.deswater.com
doi: 10.1080/19443994.2013.781739

51 (2013) 3889–3895
May

Taylor & Francis
Taylor & Francis Group

TiO_2–Au composite for efficient UV photocatalytic reduction of Cr(VI)

Xinjuan Liu, Tian Lv, Yong Liu, Likun Pan*, Zhuo Sun

Department of Physics, Ministry of Education, Engineering Research Center for Nanophotonics & Advanced Instrument, East China Normal University, Shanghai 200062, China
Tel. +86 21 62234132; Fax: +86 21 62234321; email: lkpan@phy.ecnu.edu.cn

Received 8 August 2012; Accepted 25 February 2013

ABSTRACT

TiO_2 at the nanoscale perform well in the UV photocatalytic application depending on the particle size; a combination of TiO_2 and Au may improve the situation. TiO_2–Au composites are thus synthesized and examined in the UV photocatalytic reduction of Cr(VI). Results show that the photocatalytic efficiency of TiO_2–Au reaches 91% in Cr(VI) reduction compared with the pure TiO_2 (83%) under UV light irradiation. The increased light absorption intensity in a broader spectral range as well as the rate of electron-hole pair recombination in TiO_2 with the addition of Au shall be responsible for the enhanced photocatalytic ability of the composite.

Keywords: TiO_2; Au; Composite; Photocatalysis

1. Introduction

Removal of heavy metals from both underground and surface water supplies is increasingly demanded in water purification. Among all heavy metals, Cr(VI) is toxic to most organisms when its concentration is above 0.05 mg/L and can cause irritation and corrosion of human skin. Cr(VI) is generally released from electroplating, leather tanning, metal finishing, dyeing, textiling, steel fabricating, paint and pigments, fertilizing, photographying, etc. Therefore, it is significantly important to find an effective method to remove Cr(VI) from industrial wastewaters. Various methods including adsorption [1], biosorption [2], electrocoagulation [3], ion exchange [4], and membrane filtration [5], have been widely used for the removal of Cr(VI). However, the above-mentioned technologies have some drawbacks, which still need to be overcome, such as secondary pollution in cleaning step, membrane fouling and high power consumption and expense for operation and maintenance. Therefore, the development of cost-effective and low energy consuming technology for the removal of Cr(VI) is highly desired.

Recently, considerable attentions have been paid to semiconductor oxide photocatalysis as a novel and eco-friendly technology for the removal of Cr(VI) from aqueous solutions [6–8]. Among various semiconductor oxides, TiO_2 has attracted tremendous attention as a promising candidate material owing to its intriguing optical and electronic properties, chemical stability, nontoxicity, low cost, and high activity [9–15]. However, the quick recombination of photo-induced electron-hole pairs has significantly decreased the photocatalytic performance of TiO_2. Currently, a particularly attractive option is to design and develop hybrid

*Corresponding author.

Presented at the 2012 Qingdao International Desalination Conference June 26–29, 2012, Qingdao, China

materials based on TiO_2 to solve the problem [16–19]. As a noble metal, Au exhibits unusual electric and optical properties as well as high chemical stability [20,21]. Attempts to combine TiO_2 and Au have been reported in efforts to obtain hybrid materials with excellent photocatalytic activity [22–27]. Pradhan et al. [28] prepared TiO_2–Au snowman-like heterodimer nanostructures by a surface sol–gel process based on Au nanoparticles (NPs) and found that TiO_2–Au exhibited higher photocatalytic performance in oxidation of methanol under UV light irradiation than TiO_2 NPs due to the presence of Au NPs. Hernandez-Fernandez et al. [29] reported that TiO_2–Au photocatalysts synthesized by the sol–gel method exhibited an enhanced photocatalytic performance in oxidation of nitrogen monoxide under UV light irradiation compared with pure TiO_2. Yogi et al. [30] employed a sol–gel method using polyvinyl-pyrrolidone-protected Au NPs (AuNPs@PVP) to synthesize TiO_2–Au films and found that the film doped with the smaller AuNPs@PVP and annealed at 500˚C showed the highest photocatalytic activity in photo-degradation of methylene blue under UV light irradiation due to its well-crystallized anatase phase and high adsorption ability. Wongwisate et al. [31] demonstrated that TiO_2-0.1% Au-0.1% Ag prepared by a sol–gel method displayed better photocatalytic activity in the degradation of 4-chlorophenol than TiO_2-0.1% Ag, and both of them provided the highest photocatalytic activity in terms of total organic carbon reduction. In photocatalysis process, Au NPs can act as an excellent electron-acceptor/transport material to effectively facilitate the migration of photo-induced electrons and hinder the charge recombination in electron-transfer processes due to the electronic interaction between TiO_2 and Au, which enhances the photocatalytic performance [32–35]. Despite the above progress to date, the exploration on TiO_2–Au composites, especially on their synthesis via sol–gel method and application in photocatalytic reduction of Cr(VI), is not nearly enough. In this work, one-step synthesis of TiO_2–Au composites is carried out via sol–gel method. TiO_2–Au composites exhibit an enhanced photocatalytic performance in reduction of Cr(VI) under UV light irradiation compared with pure TiO_2.

2. Experimental

2.1. Synthesis of TiO_2–Au composites

4 mL tetrabutyl titanate was first dissolved in 10 mL ethanol by stirring for 30 min at room temperature to obtain solution A. A certain amount of $HAuCl_4$ was dissolved in 7 mL ethanol, and then 2 mL deionized water and 5 mL acetic acid were successively added to the solution by stirring for 30 min at room temperature to obtain solution B. Solution B was then added dropwise into solution A under vigorous stirring. Subsequently, the mixture solution was continuously stirring at 40˚C for the hydrolysis of tetrabutyl titanate until a transparent sol was formed. Finally, the sol was dried in air at 100˚C for 24 h, grinded and heated at 500˚C for 1 h. The as-synthesized TiO_2–Au samples with 0.1, 0.3, 0.5, 0.7 wt.% Au, named as TA-1, TA-2, TA-3, and TA-4. The pure TiO_2 was also synthesized for comparison.

2.2. Characterization

The surface morphology, structure and composition of the samples were characterized by field-emission scanning electron microscopy (FESEM, Hitachi S-4800), high-resolution transmission electron microscopy (HRTEM, JEOL-2010), X-ray diffraction spectroscopy (XRD, Holland Panalytical PRO PW3040/60) with Cu Kα radiation ($V = 30$ kV, $I = 25$ mA), and energy dispersive X-ray spectroscopy (EDS, JEM-2100), respectively. The UV–vis absorption spectra were recorded using a Hitachi U-3900 UV–vis spectrophotometer. Brunauer–Emmett–Teller (BET) surface area was measured by ASAP 2020 Accelerated Surface Area and Porosimetry System (Micrometitics, Norcross, GA). The desorption isotherm was used to determine the pore size distribution using the Barret–Joyner–Halender method.

2.3. Photocatalytic experiments

The photocatalytic performance of the as-prepared samples was evaluated by photocatalytic reduction of Cr(VI) under UV light irradiation. The samples (1 g/L) were dispersed in 60 mL Cr(VI) solutions (10 mg/L) that were prepared by dissolving $K_2Cr_2O_7$ into deionized water. The mixed suspensions were first magnetically stirred in the dark for 0.5 h to reach the adsorption/desorption equilibrium. Under stirring, the mixed suspensions were exposed to UV irradiation produced by a 500 W high pressure Hg lamp with the main wave crest at 365 nm. At certain time intervals, 2 mL of the mixed suspensions were extracted and centrifugated to remove the photocatalyst. The filtrates were analyzed by recording UV–vis spectra of Cr(VI) using a Hitachi U-3900 UV–vis spectrophotometer.

The photocatalytic reaction kinetics was studied using Langmuir–Hinshelwood model. The pseudo-first-order equation is employed to fit the experimental data and can be formulated as [36]:

$$\ln(C_i/C_0) = -kt \quad (1)$$

where t and k are the photocatalysis time (min) and the reaction rate constant (min^{-1}), respectively. C_0 and C_i are the initial concentration and the concentration of Cr(VI) at time t (mg/L), respectively.

3. Results and discussion

Fig. 1(a–e) show the FESEM images of TiO_2, TA-1, TA-2, TA-3, and TA-4. It is clearly seen that all the samples display spherical particles, demonstrating that the Au loading does not leave any change in the shape of TiO_2. Furthermore, it is seen that the morphologies of samples are very rough, which may be beneficial to enhancing the adsorption of reactants and photocatalytic performance. The existence of TiO_2 in the composite is proved by the peaks of Ti and O in EDS spectra of TA-3 (Fig. 1(f)). However, no Au peak is observed, which may be due to the low amount of Au in the composite. Fig. 2(a) and (b) show the low-magnification and high-magnification HRTEM images of TA-3. Au NPs are difficult to be observed in low-magnification HRTEM image due to their low amount in the composite. However, it can be observed that a few Au NPs have been attached onto the surface of TiO_2, which plays an important role for the photocatalytic performance. Generally, the Au NPs in the composite can serve as an electron conductor, which facilitates photoelectron transfer and reduces the probability of charge recombination. However, excessive Au NPs in the composite may act the centers of electron-hole recombination and reduce the quantum efficiency, which is not beneficial to the photocatalytic performance [37].

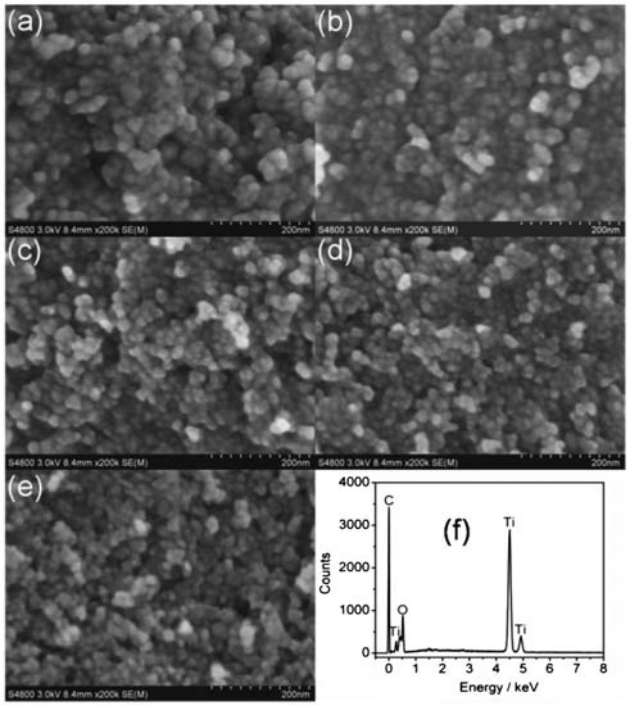

Fig. 1. Surface morphologies of (a) TiO_2, (b) TA-1, (c) TA-2, (d) TA-3, and (e) TA-4 by FESEM measurement; (f) EDS spectrum of TA-3.

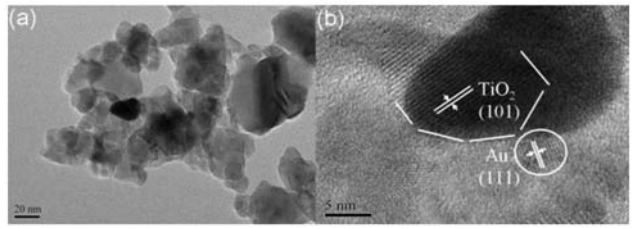

Fig. 2. (a) Low-magnification and (b) high-magnification HRTEM images of TA-3.

The XRD patterns of TiO_2, TA-1, TA-2, TA-3, and TA-4 are shown in Fig. 3. It can be seen that all the samples exhibit the diffraction peaks at 25.3˚, 37.8˚, 48.0˚, 53.9˚, 55.1˚, 62.7˚, 68.8˚, 70.3˚, and 75.0˚, indexed to (10 1), (0 0 4), (2 0 0), (1 0 5), (2 1 1), (2 0 4), (1 1 6), (2 2 0), and (2 1 5) crystal planes of anatase TiO_2 (JCPDS 21-1272), which indicates that Au loading does not result in the development of new crystal orientations of TiO_2. Compared with pure TiO_2 and TA-1, new peaks at 44.4˚, 64.6˚, and 77.6˚, corresponding to the (2 0 0), (2 2 0) and (3 1 1) planes of polycrystalline Au (JPCDS 76-1802), appear in XRD pattern of TA-2, TA-3 and TA-4, which further confirms the existence of Au in the composite. It should be noticed that the absence of Au peak for TA-1 should be ascribed to the low amount of Au below the detection limit.

Fig. 4(a) displays the BET nitrogen adsorption isotherms of TiO_2 and TA-3. The nitrogen sorption isotherm of TA-3 is similar to that of TiO_2 and belongs to the type IV behavior. The broad pore size distribu-

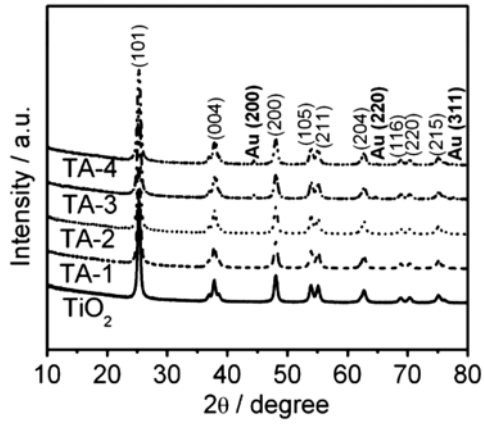

Fig. 3. XRD patterns of TiO_2, TA-1, TA-2, TA-3, and TA-4.

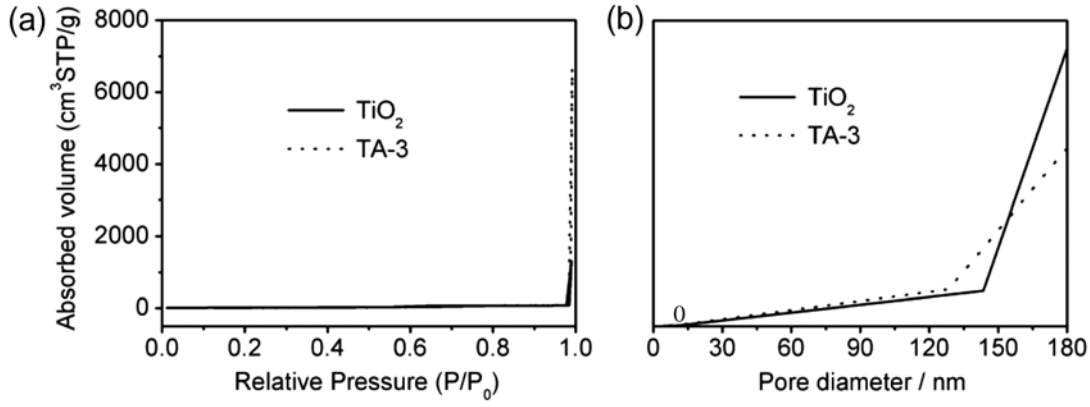

Fig. 4. (a) Nitrogen adsorption–desorption isotherms, and (b) the corresponding pore size distribution curves (inset) of TiO_2 and TA-3.

tion, as shown in the Fig. 4(b) indicates the existence of mesopores and macropores in these samples. The surface area of TiO_2 and TA-3 are 73 and 75 $m^2 g^{-1}$, respectively. The result means that the Au loading increases the specific surface area, which is beneficial for enhancing the photocatalytic activity. Furthermore, the specific surface area of TiO_2 (P25) is also characterized and the value is 54 $m^2 g^{-1}$.

The UV–vis absorption spectra of TiO_2, TA-1, TA-2, TA-3, and TA-4 are shown in Fig. 5. It is observed that TiO_2 presents its characteristic absorption peak at 330 nm and the absorbance of TiO_2–Au composite increase even in visible light region with the increase in Au content, which is similar to those reported results [33,38]. In addition, the absorption edge of TiO_2–Au composite exhibits a red shift compared to TiO_2. Similar results are also observed in other TiO_2-base composite materials [29,39,40]. Such an enhancement in the light absorption intensity and range can increase the number of photo-generated electrons and holes to participate in the photocatalytic reaction and enhance the photocatalytic performance [41].

Fig. 6 shows that the UV–vis absorbance of Cr(VI) with irradiation time under UV light irradiation using TA-3. It is observed that the UV–vis absorption peak of Cr(VI), related to the concentration of Cr(VI) in the solution, becomes weak with the increase in the time under UV light irradiation.

The photocatalytic reduction of Cr(VI) under UV light irradiation was used to evaluate the photocatalytic performance of the TiO_2, P25, TA-1, TA-2, TA-3, and TA-4, as shown in Fig. 7(a). The concentration (C) of Cr(VI) is characterized by the maximum absorption peak at about 350 nm (λ_{max}) by UV–vis spectroscopy. The photocatalytic process is demonstrated by the variation of λ_{max}. The normalized temporal concentration changes (C/C_0) of Cr(VI) during the photocatalytic process are proportional to the normalized maximum absorbance (A/A_0), which can be derived from the changes in the Cr(VI) absorption profile at a given

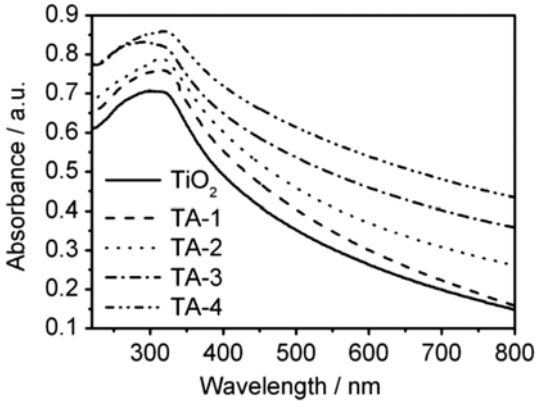

Fig. 5. UV–vis absorption spectra of TiO_2, TA-1, TA-2, TA-3, and TA-4.

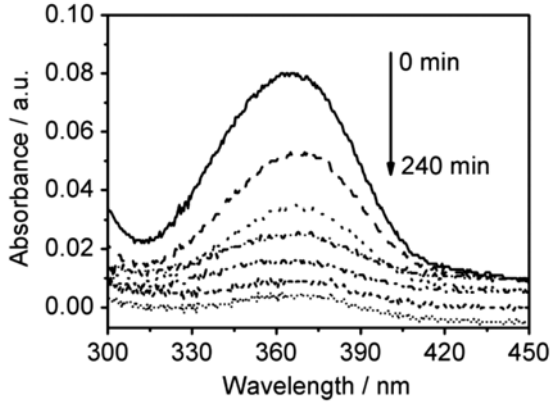

Fig. 6. The UV–vis absorbance of Cr(VI) with irradiation time during photocatalytic reduction under UV light irradiation using TA-3.

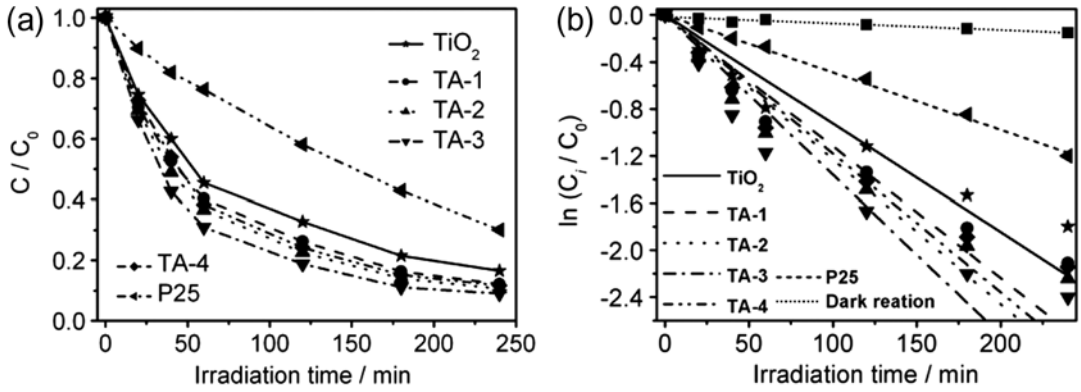

Fig. 7. (a) Photocatalytic reduction of Cr(VI) by TiO_2, P25, TA-1, TA-2, TA-3, and TA-4 under UV light irradiation; (b) The inset shows the photocatalytic reaction kinetics of Cr(VI) with reaction time. The concentrations of Cr(VI) and photocatalyst are 10 mg/L and 1 g/L, respectively.

time interval. It also can be observed that TiO_2–Au composite exhibits much higher photocatalytic performance than pure TiO_2. After 240 min, the removal rates of Cr(VI) for pure TiO_2 and P25 are calculated to be 83 and 70%, respectively. The better photocatalysis performance of TiO_2 NPs than P25 should be attributed to their higher specific surface area, which is favorable to adsorb more pollutants and separate the electron-hole pairs, thus improve the photocatalytic performance [41]. When Au is introduced into TiO_2, the removal rate is increased to 88 and 89% for TA-1 and TA-2 and reaches maximum value of 91% for TA-3 after 240 min illumination duration. Therefore, the photocatalytic performance of TiO_2–Au composite is dependent on the proportion of Au in the composite. It is known that during photocatalysis, the light absorption and the charge transportation and separation are crucial factors [42–44]. The enhancement of the photocatalytic performance should be ascribed to the increase in the light absorption intensity and range with the presence of Au in the composite and the stepwise structure of energy levels constructed in the TiO_2–Au composite, as shown in Fig. 8. The conduction band and valence band of TiO_2 are −4.2 and −7.4 eV (vs. vacuum) [45]. The work function of Au is around −5.1 eV [46]. Such energy levels are beneficial for photo-induced electrons to transfer from TiO_2 conduction band to Au, which could efficiently separate the photo-induced electrons and hinder the charge recombination in electron-transfer processes [32,47], thus enhance the photocatalytic performance. However, when the Au content is further increased above its optimum value, the photocatalytic reduction rate deteriorates. This is ascribed to the following reasons: (i) Au may absorb some UV light [33,38], and thus, there exists a light harvesting competition between TiO_2 and Au with the increase in Au

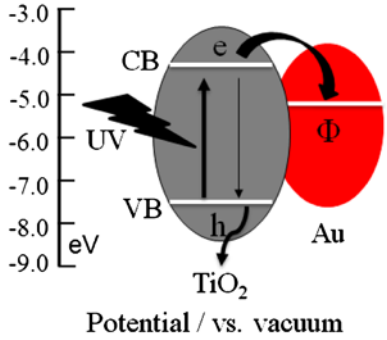

Fig. 8. Schematic diagram of energy levels of TiO_2 and Au NPs. CB and Φ are conduction band and work function.

amount, which lead to the decrease in the photocatalytic performance; (ii) the excessive Au can act as a kind of recombination center instead of providing an electron pathway and promote the recombination of electron-hole pair in Au [19,20,27].

Fig. 7(b) shows the linear fitting between pseudo-first-order kinetic equations and experimental data for TiO_2, TA-1, TA-2, TA-3, and TA-4. The values of rate constants (k) can be obtained directly from the fitted straight-line plots of $\ln(C_i/C_0)$ versus reaction time. The values of k in the dark reaction for TA-3 is 0.00057 min^{-1}, indicating that Cr(VI) can almost not be reduced in the dark reaction, which ensures the effect of physical absorption of Cr (VI) to be eliminated. Furthermore, the values of k under UV light irradiation follow the order: TA-3 (0.0136 min^{-1}) > TA-2 (0.0123 min^{-1}) > TA-4 (0.0118 min^{-1}) > TA-1 (0.0112 min^{-1}) > TiO_2 (0.0092 min^{-1}) > P25 (0.00489 min^{-1}). The result shows that TA-3 exhibits a best photocatalytic activity under UV irradiation.

4. Conclusions

TiO_2–Au composites are successfully synthesized via a simple sol–gel method and their photocatalytic

performances are investigated. The experimental results indicate that (i) TiO_2–Au composites exhibit a better photocatalytic performance than pure TiO_2; (ii) the photocatalytic performance of TiO_2–Au composite is dependent on the proportion of Au in the composite and the composite with 0.5 wt.% Au achieves a highest photocatalytic reduction rate of 91%; (iii) the enhanced photocatalytic performance is ascribed to the increase in light absorption intensity and range as well as the reduction of photoelectron-hole pair recombination in TiO_2 with the introduction of Au.

Acknowledgments

Financial support from Special Project for Nanotechnology of Shanghai (No. 1052nm02700) and Scholarship Award for Excellent Doctoral Student granted by Ministry of Education (No. MXRZZ2012006) are gratefully acknowledged.

References

[1] V.K. Gupta, S. Agarwa, T.A. Saleh, Chromium removal combining the magnetic properties of iron oxide with adsorption properties of carbon nanotubes, Water Res. 45(6) (2011) 2207–2212.

[2] G.Q. Chen, W.J. Zhang, G.M. Zeng, J.H. Huang, L. Wang, G.L. Shen, Surface-modified *Phanerochaete chrysosporium* as a biosorbent for Cr(VI)-contaminated wastewater, J. Hazard Mater. 186(2–3) (2011) 2138–2143.

[3] M.S. Bhatti, A.S. Reddy, R.K. Kalia, A.K. Thukral, Modeling and optimization of voltage and treatment time for electrocoagulation removal of hexavalent chromium, Desalination 269 (1–3) (2011) 157–162.

[4] S. Edebali, E. Pehlivan, Evaluation of Amberlite IRA96 and Dowex 18 ion-exchange resins for the removal of Cr(VI) from aqueous solution, Chem. Eng. J. 161(1–2) (2010) 161–166.

[5] W.D. Zhang, J.T. Liu, Z.Q. Ren, S.G. Wang, C.S. Du, J.N. Ma, Kinetic study of chromium (VI) facilitated transport through a bulk liquid membrane using tri-*n*-butyl phosphate as carrier, Chem. Eng. J. 150(1) (2009) 83–89.

[6] A. Idris, N. Hassan, N.S. Mohd Ismail, E. Misran, N.M. Yusof, A.F. Ngomsik, A. Bee, Photocatalytic magnetic separable beads for chromium(VI) reduction, Water Res. 44(6) (2010) 1683–1688.

[7] S.V. Awate, S.S. Deshpande, K. Rakesh, P. Dhanasekaran, N.M. Gupta, Role of micro-structure and interfacial properties in the higher photocatalytic activity of TiO_2-supported nanogold for methanol-assisted visible-light-induced splitting of water, PCCP 13(23) (2011) 11329–11339.

[8] Y. Liu, H. Wang, Y.C. Wang, H.M. Xu, M. Li, H. Shen, Substrate-free, large-scale, free-standing and two-side oriented single crystal TiO_2 nanorod array films with photocatalytic properties, Chem. Commun. 47(13) (2011) 3790–3792.

[9] W. Zhang, L.D. Zou, L.Z. Wang, A novel charge-driven self-assembly method to prepare visible-light sensitive TiO_2/activated carbon composites for dissolved organic compound removal, Chem. Eng. J. 168(1) (2011) 485–492.

[10] Y.F. Zhu, R.G. Du, W. Chen, H.Q. Qi, C.J. Lin, Photocathodic protection properties of three-dimensional titanate nanowire network films prepared by a combined sol–gel and hydrothermal method, Electrochem. Commun. 12(11) (2010) 1626–1629.

[11] Q. Shen, W. Zhang, Z.P. Hao, L.D. Zou, A study on the synergistic adsorptive and photocatalytic activities of TiO_2–xNx/beta composite catalysts under visible light irradiation, Chem. Eng. J. 165(1) (2010) 301–309.

[12] G. Li, L. Lv, H. Fan, J. Ma, Y. Li, Y. Wan, X.S. Zhao, Effect of the agglomeration of TiO_2 nanoparticles on their photocatalytic performance in the aqueous phase, J. Colloid Interface Sci. 348(2) (2010) 342–347.

[13] Z. Xiong, H. Dou, J. Pan, J. Ma, C. Xu, X.S. Zhao, Synthesis of mesoporous anatase TiO_2 with a combined template method and photocatalysis, CrystEngCommun. 12(11) (2010) 3455–3457.

[14] J.B. Lu, H. Jin, Y. Dai, K.S. Yang, B.B. Huang, Effect of electronegativity and charge balance on the visible light-responsive photocatalytic activity of non-metal doped anatase TiO2, Int. J. Photoenergy, 2012 (2012) 928503.

[15] K. Rajeshwar, C.R. Chenthamarakshan, S. Goeringer, M. Djukic, Titania-based heterogeneous photocatalysis: Materials, mechanistic issues, and implications for environmental remediation, Pure Appl. Chem. 73(12) (2001) 1849–1860.

[16] K.F. Zhou, Y.H. Zhu, X.L. Yang, X. Jiang, C.Z. Li, Preparation of graphene–TiO_2 composites with enhanced photocatalytic activity, New J. Chem. 35(2) (2011) 353–359.

[17] C.F. Lee, B.H. Chen, Y.L. Huang, Determining Cr(III) and Cr(VI) in urine using a flow injection on-line sorption separation system coupled with electrothermal atomic absorption spectrometry and a UV/nano-Au/TiO_2 photocatalysis reduction device, Talanta 77(2) (2008) 546–550.

[18] Y. Zhao, C.Z. Li, X. Liu, F. Gu, H.L. Du, L. Shi, Zn-doped TiO_2 nanoparticles with high photocatalytic activity synthesized by hydrogen–oxygen diffusion flame, Appl. Catal. B 79(3) (2008) 208–215.

[19] B.Z. Tian, C.Z. Li, F. Gu, H.B. Jiang, Synergetic effects of nitrogen doping and Au loading on enhancing the visible-light photocatalytic activity of nano-TiO_2, Catal. Commun. 10 (6) (2009) 925–929.

[20] M.V. Dozzi, L. Prati, P. Canton, E. Selli, Effects of gold nanoparticles deposition on the photocatalytic activity of titanium dioxide under visible light, PCCP 11(33) (2009) 7171–7180.

[21] Z.G. Xiong, L.L. Zhang, J.Z. Ma, X.S. Zhao, Photocatalytic degradation of dyes over graphene–gold nanocomposites under visible light irradiation, Chem. Commun. 46(33) (2010) 6099–6101.

[22] Z.K. Zheng, B.B. Huang, X.Y. Qin, X.Y. Zhang, Y. Dai, M.H. Whangbo, Facile *in situ* synthesis of visible-light plasmonic photocatalysts M@ TiO_2 (M = Au, Pt, Ag) and evaluation of their photocatalytic oxidation of benzene to phenol, J. Mater. Chem. 21(25) (2011) 9079–9087.

[23] J.J. Zhao, S. Sallard, B.M. Smarsly, S. Gross, M. Bertino, C. Boissiere, H.R. Chen, J.L. Shi, Photocatalytic performances of mesoporous TiO_2 films doped with gold clusters, J. Mater. Chem. 20(14) (2010) 2831–2839.

[24] N. Zhang, S.Q. Liu, X.Z. Fu, Y.J. Xu, Synthesis of M@TiO_2 (M = Au, Pd, Pt) core-shell nanocomposites with tunable photoreactivity, J. Phys. Chem. C 115(18) (2011) 9136–9145.

[25] A. Primo, A. Corma, H. García, Titania supported gold nanoparticles as photocatalyst, PCCP 13(3) (2011) 886–910.

[26] M. Murdoch, G.I.N. Waterhouse, M.A. Nadeem, J.B. Metson, M.A. Keane, R.F. Howe, J. Llorca, H. Idriss, The effect of gold loading and particle size on photocatalytic hydrogen production from ethanol over Au/TiO_2 nanoparticles, Nat. Chem. 3(6) (2011) 489–492.

[27] J.G. Yu, L. Yue, S.W. Liu, B.B. Huang, X.Y. Zhang, Hydrothermal preparation and photocatalytic activity of mesoporous Au–TiO_2 nanocomposite microspheres, J. Colloid Interface Sci. 334(1) (2009) 58–64.

[28] S. Pradhan, D. Ghosh, S.W. Chen, Janus nanostructures based on Au–TiO_2 heterodimers and their photocatalytic activity in the oxidation of methanol, ACS Appl. Mater. Interfaces 1(9) (2009) 2060–2065.

[29] J. Hernandez-Fernandez, A. Aguilar-Elguezabal, S. Castillo, B. Ceron-Ceron, R.D. Arizabalo, M. Moran-Pineda, Oxidation of NO in gas phase by Au–TiO_2 photocatalysts prepared by the sol–gel method, Catal. Today 148(1–2) (2009) 115–118.

[30] C. Yogi, K. Kojima, T. Hashishin, N. Wada, Y. Inada, E. Della Gaspera, M. Bersani, A. Martucci, L.J. Liu, T.K. Sham, Size effect of au nanoparticles on TiO_2 crystalline phase of nanocomposite thin films and their photocatalytic properties, J. Phys. Chem. C 115(14) (2011) 6554–6560.
[31] P. Wongwisate, S. Chavadej, E. Gulari, T. Sreethawong, P. Rangsunvigit, Effects of monometallic and bimetallic Au–Ag supported on sol–gel TiO_2 on photocatalytic degradation of 4-chlorophenol and its intermediates, Desalination 272(1–3) (2011) 154–163.
[32] X.D. Wang, R.A. Caruso, Enhancing photocatalytic activity of titania materials by using porous structures and the addition of gold nanoparticles, J. Mater. Chem. 21(1) (2011) 20–28.
[33] A. Pandikumar, S. Murugesan, R. Ramaraj, Functionalized silicate sol–gel-supported TiO_2–Au core-shell nanomaterials and their photoelectrocatalytic activity, ACS Appl. Mater. Interfaces 2(7) (2010) 1912–1917.
[34] N. Wang, T. Tachikawa, T. Majima, Single-molecule, single-particle observation of size-dependent photocatalytic activity in Au/TiO_2 nanocomposites, Chem.Sci. 2(5) (2011) 891–900.
[35] L.L. Sun, D.X. Zhao, Z.M. Song, C.X. Shan, Z.Z. Zhang, B.H. Li, D.Z. Shen, Gold nanoparticles modified ZnO nanorods with improved photocatalytic activity, J. Colloid Interface Sci. 363(1) (2011) 175–181.
[36] Y. Zhang, J.C. Crittenden, D.W. Hand, D.L. Perram, Fixed-bed photocatalysts for solar decontamination of water, Environ. Sci. Technol. 28(3) (1994) 435–442.
[37] Y. Liu, L.F. Chen, J.C. Hu, J.L. Li, R. Richards, TiO_2 nanoflakes modified with gold nanoparticles as photocatalysts with high activity and durability under near UV irradiation, J. Phys. Chem. C 114(3) (2010) 1641–1645.
[38] S.L. Luo, Y. Xiao, L.X. Yang, C.B. Liu, F. Su, Y. Li, Q.Y. Cai, G. M. Zeng, Simultaneous detoxification of hexavalent chromium and acid orange 7 by a novel Au/TiO_2 heterojunction composite nanotube arrays, Sep. Purif. Technol. 79(1) (2011) 85–91.
[39] H. Zhang, X.J. Lv, Y.M. Li, Y. Wang, J.H. Li, P25-graphene composite as a high performance photocatalyst, ACS Nano 4 (1) (2009) 380–386.
[40] Y.H. Zhang, Z.R. Tang, X.Z. Fu, Y.J. Xu, TiO_2-graphene nanocomposites for gas-phase photocatalytic degradation of volatile aromatic pollutant: Is TiO_2-graphene truly different from other TiO_2-carbon composite materials? ACS Nano 2(12) (2010) 7303–7314.
[41] M. Hamadanian, A. Reisi-Vanani, A. Majedi, Synthesis, characterization and effect of calcination temperature on phase transformation and photocatalytic activity of Cu, S-codoped TiO_2 nanoparticles, Appl. Surf. Sci. 256(6) (2010) 1837–1844.
[42] H. Zhang, X.J. Lv, Y.M. Li, Y. Wang, J.H. Li, P25-graphene composite as a high performance photocatalyst, ACS Nano 4 (1) (2010) 380–386.
[43] X.J. Liu, L.K. Pan, T. Lv, G. Zhu, T. Lu, Z. Sun, and C.Q. Sun, Microwave-assisted synthesis of TiO_2-reduced graphene oxide composites for photocatalytic reduction of Cr(VI), RSC Advance 1(7) (2011) 1245–1249.
[44] X.J. Liu, L.K. Pan, T. Lv, T. Lu, G. Zhu, Z. Sun, C.Q. Sun, Microwave-assisted synthesis of ZnO-graphene nanocomposite for photocatalytic reduction of Cr(VI), Catal. Sci. Technol. 1(7) (2011) 1189–1193.
[45] M. Gratzel, Photoelectrochemical cells, Nature 414(6861) (2001) 338–344.
[46] B. Kouskoussa, M. Morsli, K. Benchouk, G. Louarn, L. Cattin, A. Khelil, J.C. Bernede, On the improvement of the anode/organic material interface in organic solar cells by the presence of an ultra-thin gold layer, Phys. Status Solidi A 206(2) (2009) 311–315.
[47] G. Zhu, F.F. Su, T. Lv, L.K. Pan, Z. Sun, Au nanoparticles as interfacial layer for CdS quantum dot-sensitized solar cells, Nanoscale Res. Lett. 5(11) (2010) 1749–1754.